Received: 15 December 2020 | Revised: 1 March 2021 | Accepted: 3 April 2021

DOI: 10.1002/we.2642

RESEARCH ARTICLE

WILEY

Quasi-static response of a bottom-fixed wind turbine subject to various incident wind fields

Astrid Nybø[1] | Finn Gunnar Nielsen[1] | Marte Godvik[1,2]

[1]Geophysical Institute and Bergen Offshore Wind Centre (BOW), University of Bergen, Bergen, Norway

[2]R&T, Equinor ASA, Bergen, Norway

Correspondence
Astrid Nybø, Geophysical Institute and Bergen Offshore Wind Centre (BOW), University of Bergen, Allégaten 70, 5007 Bergen, Norway.
Email: astrid.nybo@uib.no

Abstract

In the design of offshore wind farms the simulated dynamic response of the wind turbine structure includes loading from turbulent wind. The International Electrotechnical Commission (IEC) standard for wind turbine design recommends both the Mann spectral tensor model and the Kaimal spectral model combined with an exponential coherence formulation. These models give deviating wind loads. This study compares these two models to a large eddy simulations model and a model based on offshore wind measurements. The comparisons are performed for three situations, covering unstable, neutral and stable atmospheric conditions. The impact of the differences in the wind fields on the quasi-static response of a large bottom-fixed wind turbine is investigated. The findings are supported by an assessment of the impact of individual wind characteristics on the turbine responses. The wind model based on measurements causes high tower bottom and blade root flapwise bending moments due to a high wind load at very low frequencies. Low and negative horizontal coherence is obtained using the Mann spectral tensor model. This causes relatively large yaw moments as compared to the results using the other wind models. The largest differences in response are seen in the stable situation. We furthermore show that the quasi-static wind load has great impact on the total damage equivalent moments of the structure. From the results, we conclude that in the design of large offshore wind turbines one should carefully consider the structure of the turbulent wind. Further, longer simulations than recommended by the standards should be used to reduce uncertainty in estimated response.

KEYWORDS

coherence, damage equivalent moments, offshore wind turbines, quasi-static response, spectral response, turbulence models

1 | INTRODUCTION

For the last decades, there has been significant yearly additions to the total installed wind energy capacity world wide.[1] In the recent years, the offshore installations are approaching a significant level, being 10% of total wind energy installations in 2019. The trend of moving offshore is driven by the available areas and superior wind conditions, but hindered by the additional complexity and costs.

In the design of offshore wind turbines, a realistic modelling of the incident wind field is important to determine the corresponding response. The recently published design standards for offshore wind turbines from the International Electrotechnical Commission (IEC)[2–4] still recommend two turbulence models initially developed for onshore small rotors in neutral atmospheric stability conditions. These are the Mann spectral tensor model, hereafter denoted 'Mann',[5] and the Kaimal spectral model combined with an exponential coherence formulation, hereafter denoted 'Kaimal'.[6] For design purposes it is common to assume that if the wind field has a given shear profile and turbulence intensity, the response of the wind turbine is not very dependent upon the spectral and coherence model used. On the contrary, previous studies[7–12] have shown that the structural loads in the response of the wind turbine are sensitive to the model chosen.

Both the research community (e.g., previous works[7,11–15]) and the industry (e.g., previous works[16]) look for improved turbulence models. They should be valid for large rotors (200 m in diameter) and account for variations in atmospheric stability conditions. The importance of a proper coherence model increases with the rotor diameter. The complexity of models are therefore increased and more site parameters are included. Several studies[7,11,12,14,17] group wind fields by stability and evaluate its impact on response. The improved certainties in the response of the offshore wind turbines may still not be worth the additional computational time and/or measurements required. In order to make the right compromise, one needs to evaluate the differences in the response using various input wind fields, and furthermore the origin of these differences.

In Nybø et al,[18] the Kaimal and Mann wind fields are compared to large eddy simulations, hereafter denoted 'LES', and wind fields based on offshore measurements, hereafter denoted 'TIMESR'. The comparisons were made for several wind speeds and atmospheric stability conditions. The current study aims to evaluate the response of a bottom-fixed wind turbine subject to the four wind spectral formulations; Kaimal, Mann, LES and TIMESR. The models are fitted to measurement situations covering stable, unstable and neutral atmospheric conditions. None of the studies mentioned above compare the responses of a wind turbine in the different wind fields presented.

In order to determine the origin of the differences in response in TIMESR, LES, Mann and Kaimal, the wind characteristics are first isolated and their effect on response evaluated. The response is evaluated in terms of damage equivalent moments, hereafter denoted as 'DEM', but more importantly the response spectra. By comparing spectral characteristics of the wind and response, it is easier to determine the origin of the response differences.

The wind induced quasi-static response (f < 0.1 Hz) is in focus, in order to exclusively study the wind impact on response. It is seen from Holtslag et al.[14] and Haaskjold et al,[7] for example, that the low-frequency region has a large impact on the overall response of bottom-fixed wind turbines. This work will furthermore show that the spectral formulations of Mann, Kaimal, LES and TIMESR vary significantly in the low-frequency region below 0.1 Hz. The uncertainty and stochastic variation in this region is furthermore assessed. To the author's knowledge, spectral analysis of the origin of differences in quasi-static response from various input wind fields has never been done before.

2 | DATA AND METHODS

2.1 | Wind fields

In this study, a number of incident wind fields are used in the analysis of a bottom-fixed wind turbine. These wind fields are introduced in Section 1 as Kaimal, Mann, TIMESR and LES. Measurements from sonic anemometers at an offshore mast outside Germany (FINO1)[19,20] are used as inputs to the various models according to Figure 1. In a previous study,[18] these wind fields are properly described and compared to each other.

In order to evaluate the wind fields, some definitions of wind characteristics are needed. The turbulence intensity, TI, is defined by the standard deviation of the wind speed in the mean wind direction, σ_u, and the mean wind speed, $\bar{u}$, according to Equation (1). In the following, TI is referred to hub height.

$$TI = \frac{\sigma_u}{\bar{u}} \tag{1}$$

According to the IEC wind turbine design standard,[2] the variation of mean wind speed with height, the wind shear, is described by the power law:

$$\bar{u}(z) = \bar{u}_{ref}\left(\frac{z}{z_{ref}}\right)^{\alpha}. \tag{2}$$

$\bar{u}$ is the mean wind speed at height z, and $\bar{u}_{ref}$ is the wind speed at a reference height, z_{ref}. α is the empirical power law exponent. As seen in Figure 1, the logarithmic law is used for the TIMESR profile. This law takes atmospheric stability into account when describing the variation of wind speed with height.

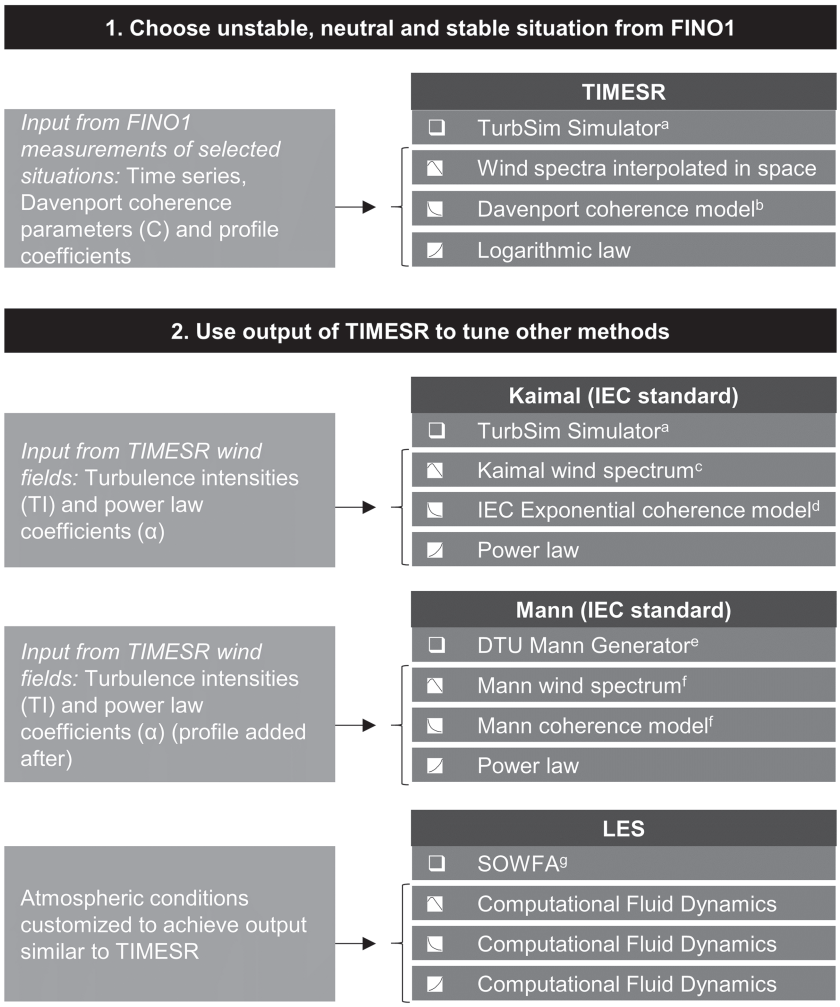

FIGURE 1 Scheme of wind field models, describing inputs, simulation software, spectra and coherence models and profile laws. a =[21], b=[22], c=[6], d=[2], e=[23], f=[5] and g=[24]

The coherence is used to quantify the correlation between the wind speed at two different locations in frequency space. Frequently, the root-coherence, or the coherence in its absolute form, is used for this purpose. The root-coherence is given by

$$|\gamma| = \frac{|S_{xy}|}{\sqrt{S_{xx}S_{yy}}}, \tag{3}$$

where S_{xx} and S_{yy} are one-sided auto-spectra of the wind velocities at two different positions, x and y, and S_{xy} is the cross spectrum between these two. The coherence, γ, may be split in a real part, the co-coherence (Re$[\gamma]$), and an imaginary part, the quad-coherence (Im$[\gamma]$). The coherence between two positions separated by a horizontal distance, δ_y, is referred to by γ_y, and a vertical distance, δ_z, by γ_z. The Davenport coherence model[22] is defined by a decay parameter, C, according to the following equation:

$$\gamma = \exp\left(-C*\frac{f\delta}{\bar{u}_m}\right), \tag{4}$$

where the frequency is represented by f and the mean wind speed between the two locations by $\bar{u}_m$. Only the coherence of the along wind component, the uu-coherence, is analysed in this work, thus in the following coherence refers to the uu-coherence if not stated otherwise. It is shown by e.g. Robertson et al.[25] that the uu-coherence is more important for the response of a 5-MW wind turbine than the vv- and ww-coherence. We assume that the u-component is still the most important when considering a larger wind turbine. It should however be noted, that the vv- and ww-coherence may have larger significance when considering several wind turbines where wake meandering matters.[26]

In Nybø et al,[18] a number of wind fields were simulated in various wind speed and stability conditions. In the present study, focus is on a wind speed just above rated in unstable, neutral and stable stratification. Further characteristics of these situations are listed in Table 1. It should be noted that the Kaimal and Mann wind fields are intended for neutral situations, so only the TI and shear is adapted when they are referred to as stable or unstable. A brief analysis of the wind speed impact on the wind turbine response is also performed, where wind fields are fitted to measurements of 7.5 and 18 m/s in neutral stratification. One hour of continuous simulation has been performed in order to properly resolve the low-frequency region.

It was a goal to achieve similar main characteristics (mean wind speed and TI at hub and shear) across models in order to easier compare differences in response due to varying formulation of wind spectra, turbulent structures and coherence. This was not fully achieved for the 12.5 m/s neutral situation, which may be observed in the range of TI in Table 1. It was challenging to achieve high enough TI in neutral conditions in LES, resulting in only 3.6%, while other models are closer to 6%. The resolution and size of the LES domain are finer and larger than given in Table 1, but interpolations are performed in order to compare at the same grounds. Figure 1 shows that TIMESR is based on measurements to a large degree. However, measurements are only conducted at a few vertical locations on the mast. The decay parameters are estimated from time series separated vertically. The decay of coherence is assumed to follow the Davenport model with equal decay parameters for horizontal and vertical separation distances. Based on the above, this model may be considered the most realistic one, but it has clear limitations and should not be considered 'true'.

Figures 2–4 show the wind spectra, co- and quad-coherence of the different simulated wind fields. For details on the spectral procedures, see Nybø et al.[18] All three figures are limited to the very low-frequency region below 0.1 Hz, where the major part of the energy and large co- and quad-coherence are observed. For the low-frequency fluctuations, only a few oscillations are achieved in the 1-hr simulations. Therefore, there is significant uncertainty associated to the spectra, co- and quad-coherence. In the calculation of these spectral properties, stationarity is assumed. TIMESR is based on 1 hr of measurements. Natural wind is not truly a stationary process, but the chosen situations are considered stationary using the criteria given in Nybø et al.[20] These criteria define stationarity based on the linear trends and moving statistics of the time series. Mann and Kaimal are stationary models, and the generated LES wind fields of this study are also found to be stationary based upon the criteria described above.[18]

In Figure 2 one observes that the energy level of the spectra decrease from unstable to stable situations (be aware of the different scales). Across stability conditions, one observes extreme values at 0.0017 Hz (lowest frequency in spectrum) for most models. Note that these values are very dependent on the block length used in the Fourier transform. With a longer block length, the extremes are moved to even lower

TABLE 1 Summary of wind field characteristics of the close to rated wind speed situation

Parameters	Unstable	Neutral	Stable
Mean wind speed at 119 m	12.6 m/s	12.4 m/s	12.5 m/s
Turbulence intensity	5.6–6.4 %	3.6–6.2 %	2.3–3.1 %
Power law exponent	0.02–0.03	0.05–0.06	0.2
	All		
Grid size horizontally and vertically	3.5 m		
Domain size horizontally and vertically	220.5 m		
Simulation time	1 hr		
Time step	0.1 s		

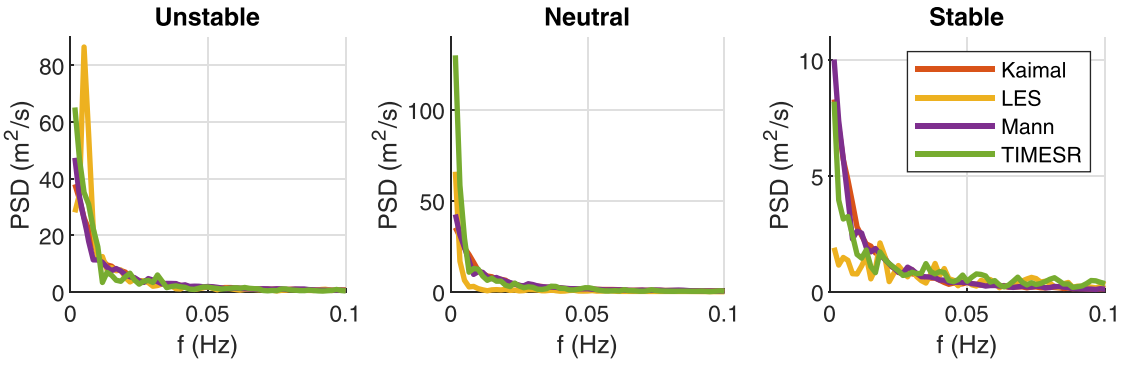

FIGURE 2 Wind spectra at 119 m for 12.5 m/s (note the different scales). The mean spectra of six 1-hr realisations are shown. PSD = Power spectral densities. Frequency step, $\Delta f = 0.0017$ Hz

frequencies, but the same trends are observed. The difference in TI between LES and other models in the neutral situation is observed in Figure 2 (middle). The power spectral densities of LES are lower than of other models, especially in the region 0.0033–0.04 Hz. The wind spectra of Mann and Kaimal are very similar, as the Mann inputs are customized to fit the Kaimal spectrum according to the IEC wind turbine design standard.[2]

Figures 3 and 4 show the co- and quad-coherence at 0.7D separation distance normal to the wind direction of wind turbines with about 180- and 80-m diameter, respectively. Distances in the order of the diameter of the wind turbine are assumed to be most relevant for tower response. Figure 3 is therefore most relevant for the analysis of the DTU 10 -MW wind turbine, while Figure 4 is rather relevant for wind turbines common

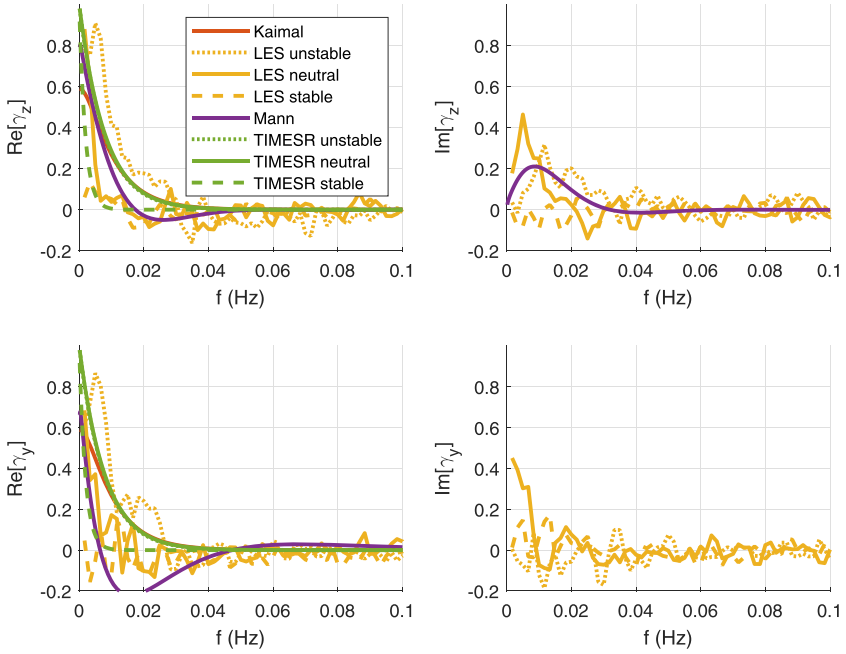

FIGURE 3 Co- (left) and quad-coherence (right) with 0.7D vertical (top) and horizontal (bottom) separation distances for wind fields of 12.5 m/s and neutral atmospheric conditions. D=178.3 m (DTU 10-MW reference turbine)

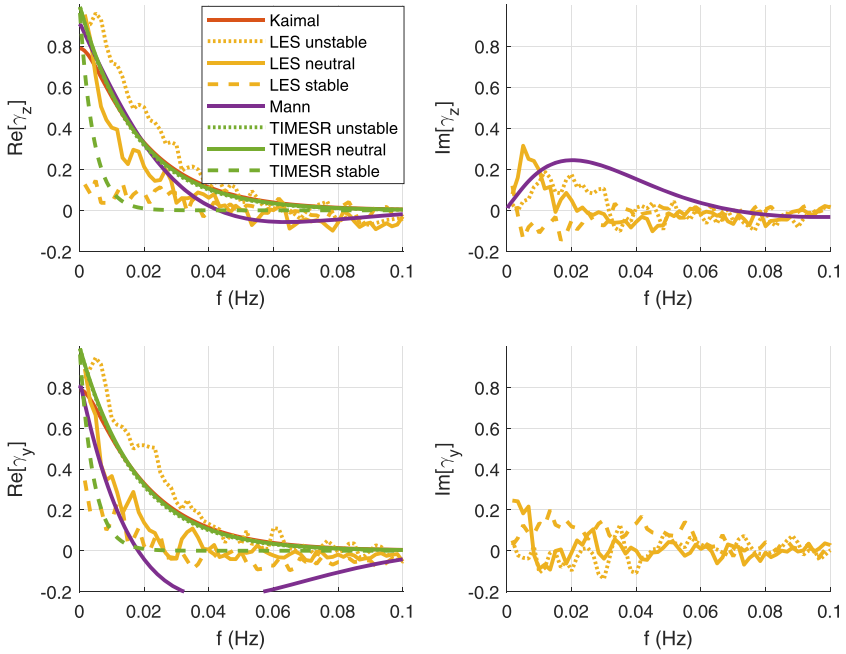

FIGURE 4 Co- (left) and quad-coherence (right) with 0.7D vertical (top) and horizontal (bottom) separation distances for wind fields of 12.5 m/s and neutral atmospheric conditions. D=80 m (1–2 MW)

20 years ago. The two figures show that a wind field hitting a large wind turbine is less coherent than the wind field hitting a smaller turbine. One observes that the co- and quad-coherence are close to zero over about 0.05 Hz in Figure 3. The comparison of Figures 3 and 4 shows that the importance of a proper coherence model increases with the rotor diameter, and design standards must be updated accordingly.

The co-coherence is higher in unstable situations than stable, clearly shown by LES in Figures 3 and 4. The stable TIMESR co-coherence is also decaying fast with frequency, but the neutral and unstable values of co-coherence are rather similar. The chosen unstable and neutral situations are in general very similar, also shown by Table 1, Figure 2 and Nybø et al.[18] Nybø et al.[18] found increasing co-coherence with increasing wind speed. In the literature, it is common to focus on the positive co-coherence for wind turbine purposes.[2,27–29] However, significant negative co-coherence and non-zero quad-coherence are observed in LES and Mann in Figures 3 and 4. The corresponding phase shifts between two time series separated in space are expected to influence the quasi-static response of a wind turbine. The quad-coherence is typically significant at frequencies where the co-coherence lies between zero and unity.

2.2 | Response

A slightly modified version of the DTU 10-MW reference turbine is used in the present study.[30] The modifications on the turbine itself are performed by Bachynski and Ormberg,[31] while Sørum et al.[32] designed the monopile foundation. The wind turbine, foundation and soil characteristics used in the current study are equal to the base model of Sørum et al,[32] with the exception of a slightly larger monopile diameter. The water depth is 30 m and the monopile extends 43 m below the mud line. The lowest point of the monopile is fixed in all degrees of freedom. The wind turbine has a hub height of 119 m and a diameter of 178.5 m. The lowest natural frequencies are the 1st tower side-side and fore-aft modes at about 0.23 Hz. At 12.5 m/s, the first excitation frequency, 1P, is 0.16 Hz. All natural frequencies and excitation frequencies are thus higher than the low-frequency region ($f < 0.1$ Hz) in focus in the present study. This region shows exclusively the quasi-static response as all natural frequencies are well above the frequency range considered.

During operation, large dynamic loads are expected close to the rated wind speed, 11.4 m/s. To stay above, but close to the rated wind speed, 12.5 m/s is chosen as the mean wind speed. From the simulation results it is observed, with a few exceptions, that the power output is constant at 10 MW throughout the duration of the simulations. For the TIMESR simulations in neutral atmospheric conditions the power drops below 10 MW in 3%–5% of the simulation time. This can be attributed to the high power density of the wind spectra at very low frequencies. The filter frequency for the generator speed controller is set to 0.2 Hz; thus, the control system is active in the low-frequency region.

The aero-hydro-servo-elastic tool SIMA[33] is used for the wind turbine simulations. The aerodynamic loads are calculated with the blade element momentum theory. The simulations are performed with a time step of about 0.01 s and a total length of 3800 s. The last hour of the simulations is used for analysis, reserving the initial 200 seconds for transient effects to die out.

For details on the number of SIMA runs conducted for this study, see Table 2. Simulations with specific wind characteristics, referred to in Table 2 under 'Wind characteristics tests', are run in order to evaluate the effect of shear, turbulence and coherence independently. The simulations referred to under 'Wind characteristics tests' are all discussed in Section 3.3. Some of them are run with only one realisation as their characteristics differ distinctly, while others require higher certainty. The wind fields of Kaimal, Mann and TIMESR are run with six different realisations, further discussed in the statistical analysis of Section 3.2. The mean characteristics of the six TIMESR realisations are used as inputs to the six Kaimal and Mann realisations. LES is only run with one realisation per stability and wind speed due to the computational efforts required.

The tower top yaw moment, hereafter denoted M_z, the tower top bending moment fore-aft, $M_{T,y}$, the tower bottom bending moment fore-aft, $M_{B,y}$, and the blade root flapwise bending moment, M_F, are considered in the response analysis. Only the dynamic response is considered, thus any reference to response corresponds to the dynamic response. Mean values have not been assessed. The mentioned responses are impacted by different characteristics in the wind. $M_{B,y}$ and M_F are, for example, expected to be large if the wind turbine is subject to a fully coherent wind field over the rotor, while M_z and $M_{T,y}$ will be larger if there are large variations in the wind field. Horizontal variations in the wind field is expected to influence the yaw moment while vertical variations may influence the fore-aft moments. The flapwise bending moment is, on the other hand, expected to be less dependent on direction. The fore-aft moments are expected to be far larger than the side-side moments, thus the side-side moments are not considered any further in this study.

The response is evaluated in terms of spectra and DEM. The response spectra are estimated using Welch's algorithm[34] with a Hamming window, six segments, and 50% overlapping. The standard deviation of the response time series, for example, used by Haaskjold et al.[7] also indicates the damage experienced by the wind turbine. However, it only takes into account the amplitudes of the response, without accounting for the number of oscillations. The DEM, R_{eq}, takes into account the amplitudes of the time series, R_i, the number of cycles, n_i, and the Wöhler curve exponent of the material, m, according to Equation (5).[35]

$$R_{eq} = \left(\frac{\Sigma_i (R_i^m n_i)}{n_{eq}} \right)^{1/m} \tag{5}$$

TABLE 2 Summary of simulated wind fields, number of realisations and SIMA runs

Method	Number of wind realisations and SIMA runs	
Wind characteristics tests		
Uniform wind		1
Sheared wind		1
Turbulent sheared wind with $\gamma = 1$		1
Turbulent sheared wind with $\gamma_y = 1$		1
Turbulent sheared wind with $\gamma_z = 1$		1
Turbulent sheared wind with $\mathrm{Im}[\gamma_z] \neq 0$		6
Turbulent sheared wind with $\mathrm{Im}[\gamma_z] = 0$		6
Turbulent sheared wind allowing for $\mathrm{Re}[\gamma_y] < 0$		6
Turbulent sheared wind replacing $\mathrm{Re}[\gamma_y] < 0$ by 0		6
Turbulent sheared wind replacing $\mathrm{Re}[\gamma_y] < 0$ by $\lvert\mathrm{Re}[\gamma_y]\rvert$		6
Response analysis		
Kaimal	12.5 m/s:	6 per stability
	7.5 and 18 m/s:	1
LES		1 per stability and wind speed
Mann	12.5 m/s:	6 per stability
	7.5 and 18 m/s:	1
TIMESR	12.5 m/s:	6 per stability
	7.5 and 18 m/s:	1

The rainflow algorithm developed by Nieslony[36] is used to compute the DEM, where half-cycles are weighted as $n_i = 0.5$. This practice is recommended by the IEC standard.[35] It is shown by Stewart et al.[37] that there may be large differences in fatigue damage with simulation length, depending on the way half-cycles are treated. In the same article, it is shown that weighting half-cycles as 0.5 results in less sensitivity to simulation length than ignoring them or counting them as full cycles. n_{eq} is the equivalent number of response cycles, in this case for an equivalent frequency of 1 Hz. For the Wöhler curve exponent, 10 (composite material) is used for calculating the blade equivalent moment, and 3 (steel) for calculating the tower equivalent moments.

In order to evaluate the response from the low-frequency region exclusively, the time series are low-pass filtered at 0.1 Hz. The high-frequency components of the fast Fourier transform of the original time series are cut. The low-pass filtered time series are thereafter produced by inverse Fourier transformation. To avoid distortions of the ends of the filtered time series, a leader/trailer corresponding to 10% of the initial time history is introduced before applying the FFT. The leader/trailer is a mirror of the beginning/end of the time series linearly ramped off to zero. The low-pass filter is applied in a region of low gradients.

The focus of this study is on the aerodynamic loads, thus no waves or current are present in the simulations. By including aligned waves typical for the North Sea (H_s=3.2 m and T_p=8.8 s), it was observed that the waves had negligible impact on the DEM of M_z, $M_{T,y}$ and M_F. The contribution to the DEM of the wind alone was about 70% of the total DEM for $M_{B,y}$. Waves are not considered further as the aim of this work is to investigate the importance of the low-frequency wind loads.

3 | RESULTS AND DISCUSSION

3.1 | Importance of the low-frequency region

This study focuses on the quasi-static response at frequencies below 0.1 Hz. In the following, we illustrate the importance of this low-frequency region on the total response.

From the response spectra, one may observe the frequency dependent amplitudes, but it is not straight-forward to interpret the dependence of the number of oscillations. In Figure 5 (left), one observes the spectrum of the M_z with a Kaimal wind field input. There are high peaks at low frequencies, but given the few oscillations of these cycles, their impact on DEM is not as high.

In order to evaluate the importance of the low-frequency region on the total damage, a low-pass filter at a number of frequencies on the original time series is used. This gives the cumulative contribution to DEM, as shown in Figure 5 (middle). This plot converges to the DEM of the

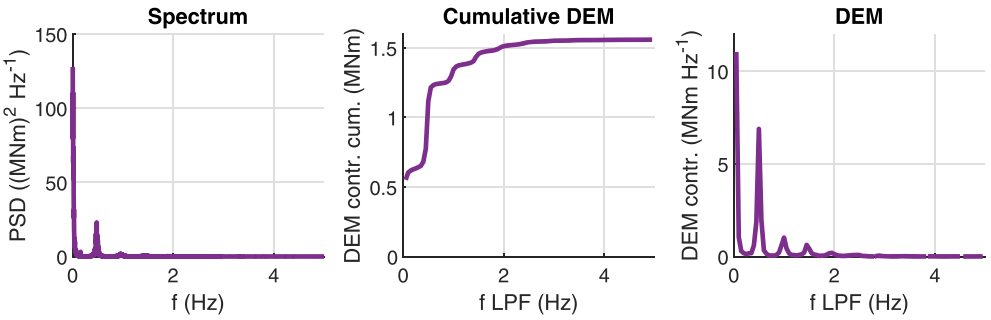

FIGURE 5 Overview of procedure for determining frequency-dependent damage equivalent moment (DEM). f LPF is the cutoff frequency in the low-pass filter. Contr. = contribution, cum. = cumulative. A Kaimal wind field of about 12.5-m/s mean wind speed is used

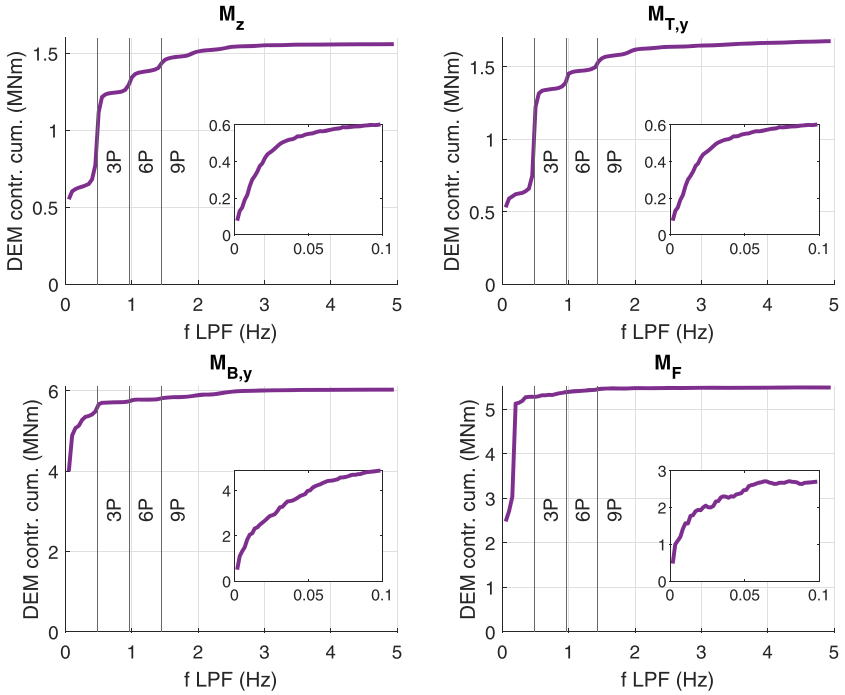

FIGURE 6 Cumulative contribution to DEM of a Kaimal wind field with a mean wind speed of about 12.5 m/s. f LPF is the cutoff frequency in the low-pass filter (0.05 Hz for the large plots and 0.0017 Hz for the smaller boxes), contr. = contribution, cum. = cumulative

original time series. The gradient of the cumulative contribution provides the frequency dependent contribution to DEM shown in Figure 5 (right). This method is further explained by Bergami and Gaunaa.[38] The low-pass filter described above is used with intervals of 0.05 Hz. As it is applied even in regions of high gradients, distortions may appear. Still, expected results are observed, similar to the spectra, but with higher impact from higher frequencies. The obtained frequency dependent DEM is dependent on the low-pass filter chosen; thus, the results should be considered qualitatively, not quantitatively.

Figure 6 shows the cumulative contribution to DEM for all considered responses using the same Kaimal input wind field. It shows that low frequencies are very important for $M_{B,y}$ and M_F. Large eddies covering most of the rotor area cause large tower bottom and blade root moments, for example for M_F almost all damage is caused by responses below 0.25 Hz. In contrast to the tower response, the blade response is strongly influenced by the 1P frequency at about 0.16 Hz. Smaller eddies at higher frequencies covering only a small fraction of the rotor area have more significant impact on the tower top moments. For M_z and $M_{T,y}$ the responses at the blade passing frequency, 3P as well as the multiples, 6P and 9P, contribute significantly to the damage. However, the quasi-static response at the lowest considered frequency is the largest single contributor to the DEM of all the four responses considered when considering frequency intervals of 0.05 Hz shown by the large plots of Figure 6.

It should be highlighted again, that there are large uncertainties associated with the low-frequency region of the wind spectra, the coherence and the response spectra. These uncertainties are reduced by using not too short block lengths in the FFT, long time series, and several realisations of these as discussed in Section 3.2.

3.2 | Statistical reliability of the quasi-static response

The IEC wind turbine standard[2] states that the total period of wind data should be long enough to ensure statistical reliability. More specifically, at least 1 hr of simulation should be run. To investigate whether the IEC recommendation is robust enough for comparison of turbulence models, specifically in the low-frequency region, the following analysis is performed.

First, it should be mentioned that the wind fields generated in this study are assumed to be stationary, as discussed in Section 2.1. However, Figure 2 shows that the time duration considered is not much longer than the duration of the large energy containing eddies. Therefore, the wind fields considered cannot be considered truly stationary. The small boxes of Figure 6 show that frequencies below 0.1 Hz matter significantly to the total DEM, but also that the very lowest frequencies considered (e.g., below 0.01 Hz) are not at all dominant for the total DEM. Due to limited contribution from the very low frequencies, the non-stationarity of the wind fields is assumed to have minor effect on the results.

The stochastic variation of the response time series may be evaluated in terms of the relative variance. Bendat and Piersol[39] show that the relative variance is inversely proportional to the bandwidth of the process, B, and the duration of the time series, T. For a boxcar power spectral density function, the relative variance is given by:

$$\frac{var[\hat{\psi}^2]}{\psi^4} \approx \frac{1}{BT}, \tag{6}$$

where $\hat{\psi}^2$ is the estimated variance of each simulated time series, while ψ^2 is the variance achieved by an infinite number of simulations. ψ^4 is estimated by using the square of the mean variance of the simulated time series. As the spectra are not boxcar shaped in the present case and the convergence of Equation (6) is slow with respect to the number of realisations needed, the result is used in a qualitatively sense.

A comparison between the relative variance (Equation (6)) of the total response time series and the low-frequency one is performed for 1 hr simulation split in six 10-min time series. The comparison confirms that the stochastic variation is stronger when considering only the low frequencies (not shown). In this section, the standard recommendation is thus compared towards a six times longer time series, hereby referred to as follows:

- '60MIN': Six simulations of duration 60 min. Each with different seed number and thus considered statistically independent.
- '10MIN': One of the above 60-min series are split into six 10-min series (IEC standard). These 10-min series are also assumed statistically independent.

Assuming a bandwidth limited Gaussian process, one should expect the relative variance to be inversely proportional to the simulation time, Equation (6), i.e the relative variance for the 10MIN should be about six times larger than that of the 60MIN. In Table 3, the relative variance of 10MIN is divided by the relative variance of 60MIN. For all responses and wind fields considered, the uncertainty is significantly reduced by increasing the total time by a factor 6. For most wind fields, the reduction is higher for $M_{B,y}$ and M_F than M_z and $M_{T,y}$. The values shown represent the mean of using six different 60-min realisations in the 10MIN relative variance. As mentioned, there is large uncertainty in the relative variance. This is observed by large variations among the different realisations (not shown). The reduction in uncertainty with duration shown by the relative variance in Table 3 is reflected in the DEM, as explained below.

TABLE 3 $\frac{var[\hat{\psi}^2]}{\psi^4}_{10MIN} \Big/ \frac{var[\hat{\psi}^2]}{\psi^4}_{60MIN}$ for the response time series

	M_z	$M_{T,y}$	$M_{B,y}$	M_F
TIMESR	3.9	2.0	45.3	24.4
$\text{TIMESR}_{\text{LPF}}$	3.9	1.6	45.8	32.8
Kaimal	35.1	5.9	14.9	33.2
$\text{Kaimal}_{\text{LPF}}$	27.2	7.8	14.4	17.3
Mann	10.0	2.9	14.9	4.2
Mann_{LPF}	6.9	4.3	14.3	20.3

Note: LPF = low-pass filtered at 0.1 Hz.

Figure 7 shows the various response spectra, using wind fields according to Kaimal, Mann, TIMESR and LES in neutral stability conditions. The spectra of $M_{B,y}$ and M_F are narrower than $M_{T,y}$ and M_z. The lower bandwidths cause higher uncertainty in the relative variances. The response dependent uncertainty may also be observed in Figure 8. This figure shows the low-frequency DEM of the various input wind fields. The ranges in strong colors represent the stochastic variation (60MIN) from the minimum value to the maximum value of the six realizations. In agreement with the bandwidths, there are larger ranges at the tower bottom and blade root than at the tower top. Figure 8 also shows the stochastic variation of 10MIN in black lines. The reduced range going from 10MIN to 60MIN illustrates the reduced stochastic variability when increasing the total duration of simulation.

From Figure 8 it is observed that the stochastic variations between results from individual realizations (range in dark colors) may be larger than the differences between turbulence models. This is, for example, the case for Mann and Kaimal at M_F in the 12.5-m/s situation. From the mean values, shown by white lines, one observes that Kaimal leads to significant higher damage than Mann. However, if running only 1 realization of 3600 s, we could have achieved opposite results. This confirms that we need several 1-hr simulations in order to achieve reliable results for comparisons of the low-frequency responses.

To sum up, there is a stronger stochastic variation when focusing exclusively on the low-frequency region, which is compensated by more simulations. This is necessary in order to achieve higher certainty when comparing the DEM of the various input wind fields. It is furthermore seen that the stochastic variation is higher at the tower bottom and blade root than at the tower top.

3.3 | Expected impact of shear, turbulence and coherence

The individual impact of shear, turbulence level and coherence on the different responses are considered in the following. The impact of coherence of vertical and horizontal separation distances is considered separately, with a special focus on quad-coherence and negative co-coherence. The different wind fields considered are described in Table 4. All the wind fields have close to rated wind speed at hub height.

No impact from shear on the response for frequencies below 0.1 Hz is expected. Figure 9 shows the spectra of the responses corresponding to the wind fields W1–W6. Comparing W1 (uniform flow) and W2 (shear flow), it is observed that the sheared wind field enhances responses at 3P for the tower moments and 1P for the blade moment. For other frequencies, no significant differences are observed. When no turbulence is present, only the rotor frequencies (1P, 3P) and multiplies of these (6P, 9P,...) contribute to the damage of the wind turbine.

Adding turbulence to the wind field, the distinct narrow peaks at e.g. 3P of the W1 and W2 spectra are becoming less distinct. Except for this, the responses generally increase in the whole frequency range, and in particular in the low-frequency region, below 0.1 Hz.

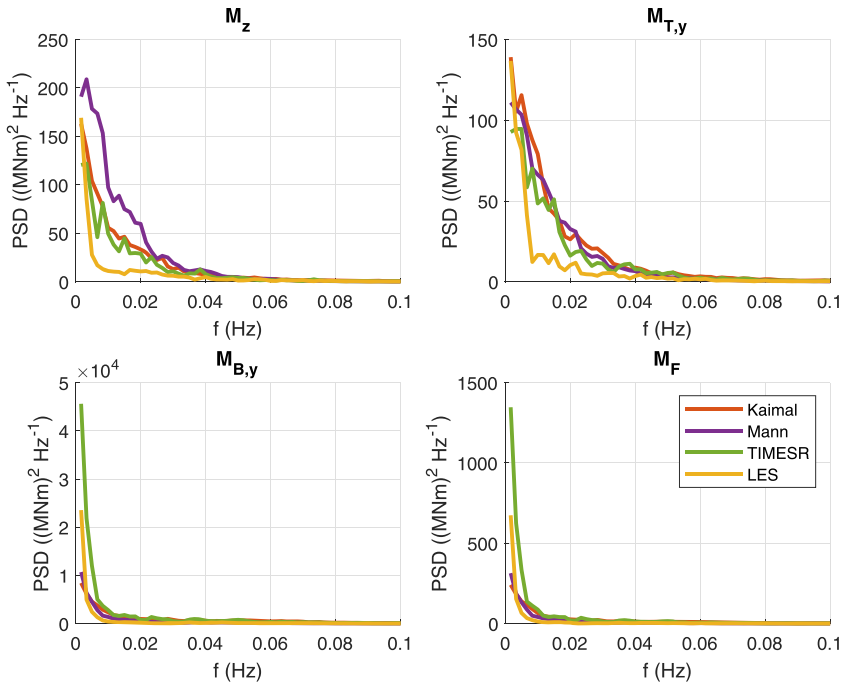

FIGURE 7 Response spectra of the wind turbine subject to wind fields of 12.5 m/s and neutral atmospheric conditions. The mean spectra of six 1-hr realisations are shown. PSD = Power spectral densities. Frequency step, Δf = 0.0017 Hz

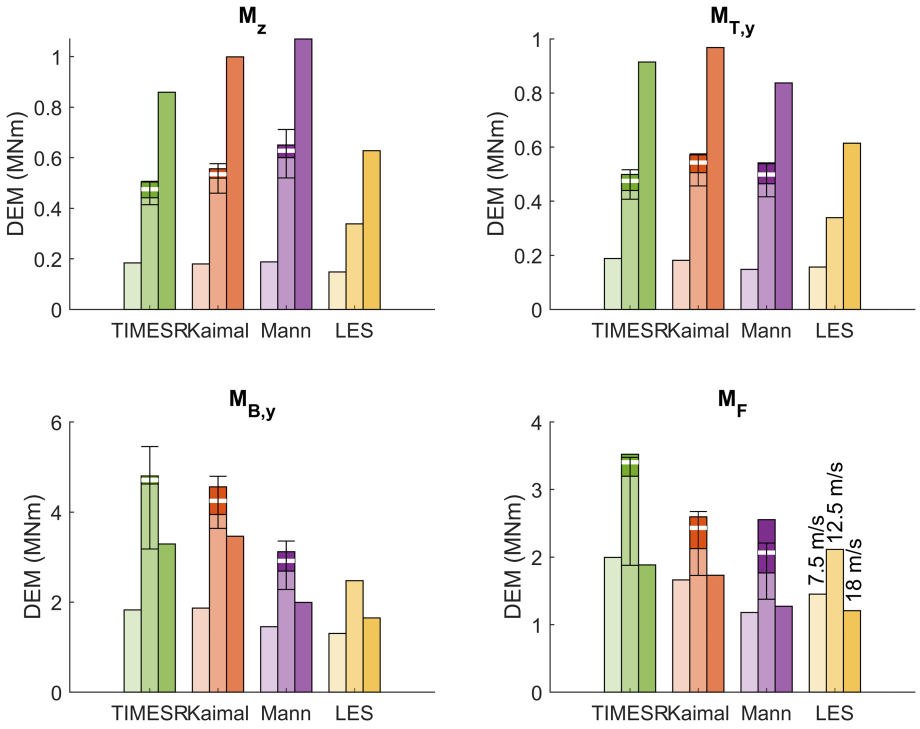

FIGURE 8 Damage equivalent moments of the low-pass filtered response time series for three input wind speeds. For 12.5 m/s, the mean (white lines) and the range (dark colors) of six 1-hr realisations (60MIN) are shown, in addition to the range (black lines) of six 10-min realisations (10MIN)

TABLE 4 Wind fields used in studying the various contributions to turbine loads. Mid rules separate different generation techniques where the first block is generated in SIMA, the second is based on a TurbSim Kaimal wind field and the third is generated from a slightly modified version of Cheynet's generator

Code	Wind field	α	TI	Same TS in hor. cells	Same TS in ver. cells + shear	Description
W1	Uniform wind	0	0%	yes	yes	
W2	Sheared wind	0.06	0%	yes	yes	
W3	Turbulent sheared wind with $\gamma = 1$	0.06	6%	yes	yes	TS from hub height Kaimal wind field (W6).
W4	Turbulent sheared wind with $\gamma_y = 1$	0.06	6%	yes	no	TS from mid Kaimal wind field (W6).
W5	Turbulent sheared wind with $\gamma_z = 1$	0.06	6%	no	yes	TS from mid Kaimal wind field (W6).
W6	Kaimal	0.06	6%	no	no	According to the IEC standard.
W7	Turbulent sheared wind with $\mathrm{Im}[\gamma_z] \neq 0$	0.06	6%	yes	no	Kaimal spectrum with Davenport $\mathrm{Re}[\gamma_z]$ (arbitrary C's) and $\mathrm{Im}[\gamma_z]$ from Equation (7), with $C_1 = 5$ and $C_2 = 10$.
W8	Turbulent sheared wind with $\mathrm{Im}[\gamma_z] = 0$	0.06	6%	yes	no	Same as W7, but C_1=0 and C_2=0.
W9	Turbulent sheared wind allowing for $\mathrm{Re}[\gamma_y] < 0$	0.06	6%	no	yes	Kaimal spectrum with $\mathrm{Re}[\gamma_y]$ from Equation (8), with $C_3 = 4\pi$, $C_4 = 5$ and $C_5 = 0.035$.
W10	Turbulent sheared wind replacing $\mathrm{Re}[\gamma_y] < 0$ by 0	0.06	6%	no	yes	Same as W9, but $\mathrm{Re}[\gamma_y] < 0$ replaced by 0.
W11	Turbulent sheared wind replacing $\mathrm{Re}[\gamma_y] < 0$ by $\lvert\mathrm{Re}[\gamma_y]\rvert$	0.06	6%	no	yes	Same as W9, but $\mathrm{Re}[\gamma_y] < 0$ replaced by positive equivalent.

Note : Hor. = horizontal and ver. = vertical

A wind field with high co-coherence over the rotor as compared to a wind field with low co-coherence, causes lower moments at the tower top and higher moments at the tower bottom and blade root. Low coherence is associated with large variations in the wind velocity over the blades, causing significant local moments. Figure 9 shows that low horizontal co-coherence (W5) causes significant M_z, while low vertical co-coherence (W4) causes high $M_{T,y}$. These observations are in agreement with the findings of Putri et al. and Doubrawa et al.[11,12] A simplified illustration showing the impact of the co-coherence on response is given in Figure 10. 'A' is a simplified version of W5, 'B' of W4 and 'C' of W3, while 'D' shows the situation at higher frequencies. Wind fields with low correlation of the wind speed (W4, W5 and W6) over the rotor area, either vertically or horizontally, cause reduced total loads on the rotor, which again reduce $M_{B,y}$. On the contrary, a co-coherence approaching one implies that the forces on the rotor blades act in phase and thus create a large $M_{B,y}$. Similarly, the M_F will be large. Although not shown in Figure 9, a wind field with very low coherence for all separation distances are expected to cause low local and global moments, as illustrated by 'D' in Figure 10.

The impact of quad-coherence is found to be almost negligible from comparisons of W7 and W8. The largest difference is found at the tower bottom, where $M_{B,y}$ is increased by 3% when accounting for quad-coherence. To include quad-coherence, the Davenport model (Equation (4)) is supplied by an imaginary part as proposed by Cheynet.[40] The quad-coherence for a vertical separation distance, δ_z, is generated according to

$$\mathrm{Im}[\gamma_z] = C_1 * \frac{f * \delta_z}{\bar{u}} * \exp\left(-C_2 \frac{f * \delta_z}{\bar{u}}\right). \tag{7}$$

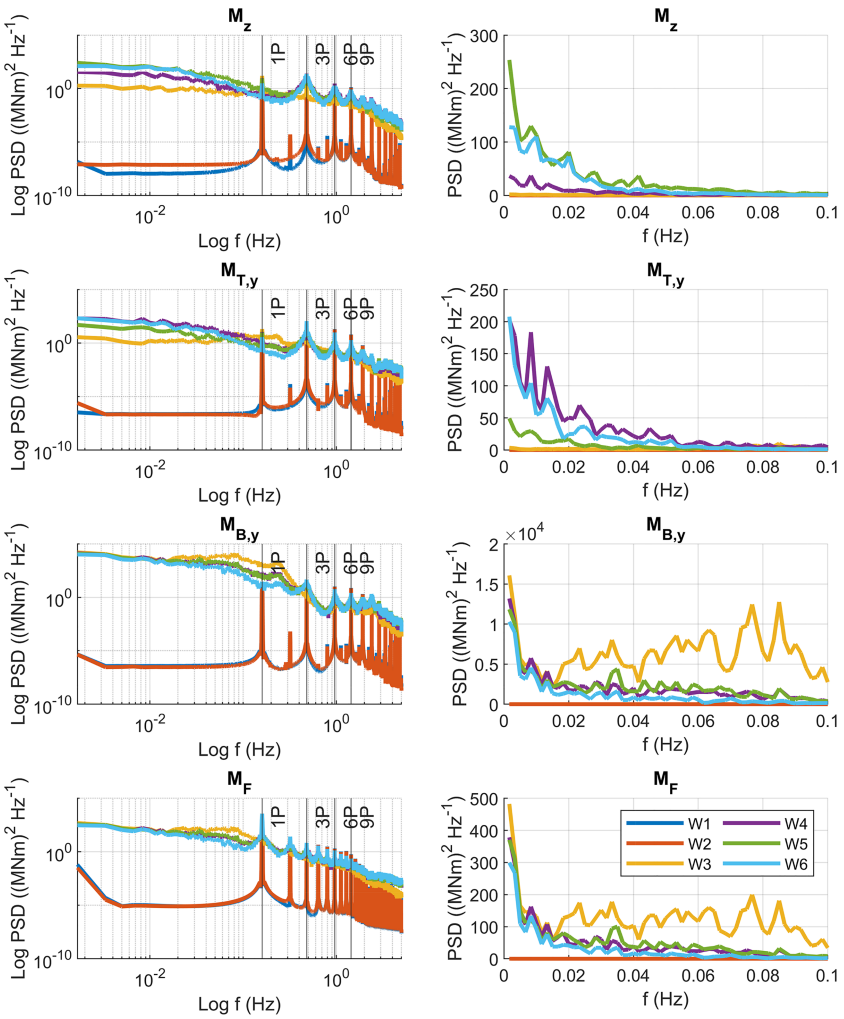

FIGURE 9 Response spectra of wind turbine response using wind fields W1-W6 of Table 4. Responses plotted using double logarithmic scale to the left; to the right the low-frequency response ($f < 0.1$ Hz) is plotted using linear scales. PSD = Power spectral densities. Frequency step, $\Delta f = 0.0017$ Hz

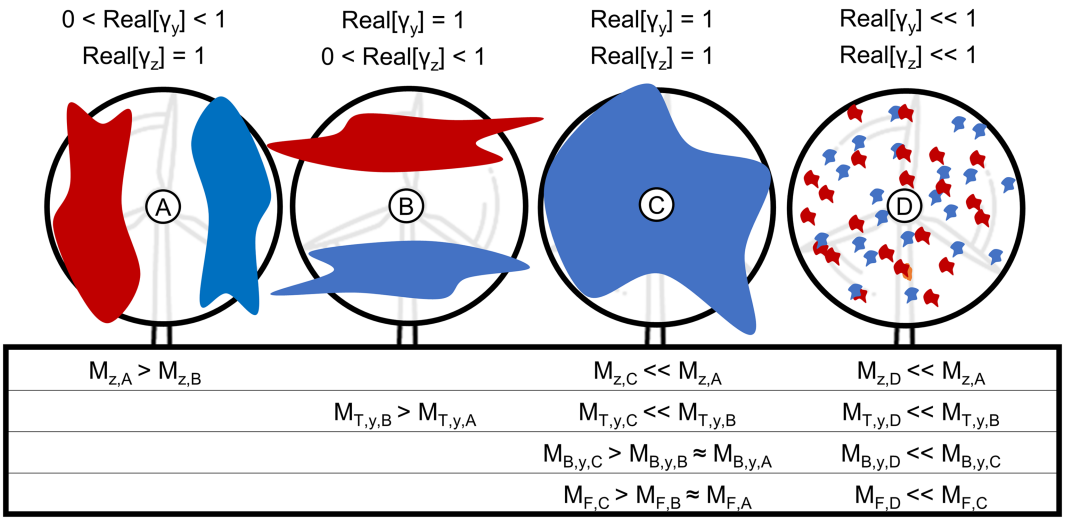

FIGURE 10 Illustration of the impact of co-coherence and eddy size on response. Different colors represent uncorrelated eddies. M refers to the dynamic moments

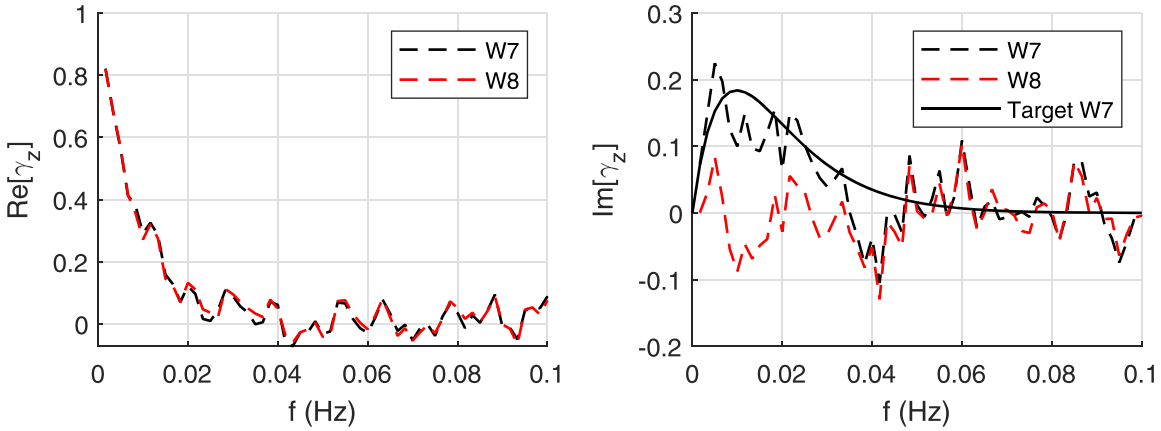

FIGURE 11 Co- (left) and quad-coherence (right) with 0.7D of DTU 10-MW vertical separation distance of the wind fields W7 & W8 of Table 4. The mean coherence of six 1-hr simulations are shown

With the decay parameters, C_1 and C_2, given in W7 of Table 4, the quad-coherence obtained is similar to Mann and lower than LES, as shown in Figure 11. The quad-coherence of the Mann and LES wind fields considered in this study is thus expected to have minor importance for the M_z, $M_{T,y}$, $M_{B,y}$ and M_F.

Keeping the negative co-coherence causes lower moments at the tower bottom and somewhat increased yaw moments in the low-frequency range as compared to the moments obtained when replacing the negative co-coherence with the absolute value or zero. The negative co-coherence for a horizontal separation distance, δ_y, is generated according to the principles outlined by Cheynet:[41]

$$\mathrm{Re}[\gamma_y] = \cos\left(C_3 * \frac{f * \delta_y}{\bar{u}}\right) * \exp\left(-\frac{\delta_y * \sqrt{(C_4 * f)^2 + C_5^2}}{\bar{u}}\right). \tag{8}$$

With the decay coefficients, C_{3-5}, given in W9 of Table 4, the negative co-coherence is similar to Mann. The co-coherence of wind fields W9-W11 is shown in Figure 12, and its corresponding impact on the response spectra in Figure 13. Keeping the negative co-coherence (W9) rather than using the absolute value (W11), increases the M_z and $M_{T,y}$ in the same frequency range where the co-coherence of W9 and W11 differ (considering a separation distance of 0.7D). As may be expected, M_z is stronger influenced by the negative horizontal co-coherence than the fore-aft moment. Keeping the negative co-coherence (W9) causes increased local moments in the top of the turbine, but reduces the total horizontal force at the tower top, causing lower moments at the bottom of the tower. Across responses, the differences in co-coherence

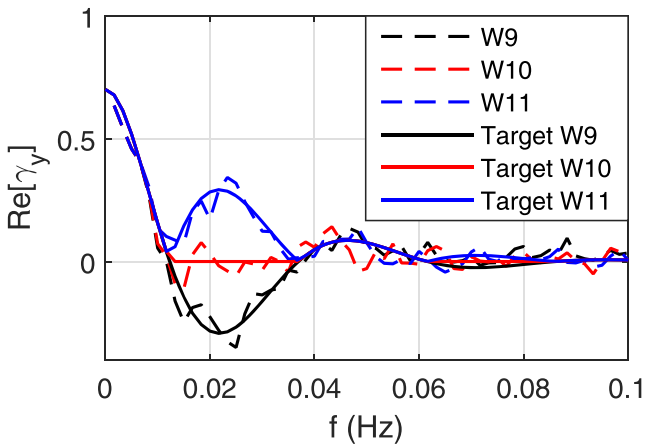

FIGURE 12 Co-coherence with 0.7D of DTU 10-MW horizontal separation distance of the wind fields W9-W11 of Table 4. The mean co-coherence of six 1-hr simulations are shown

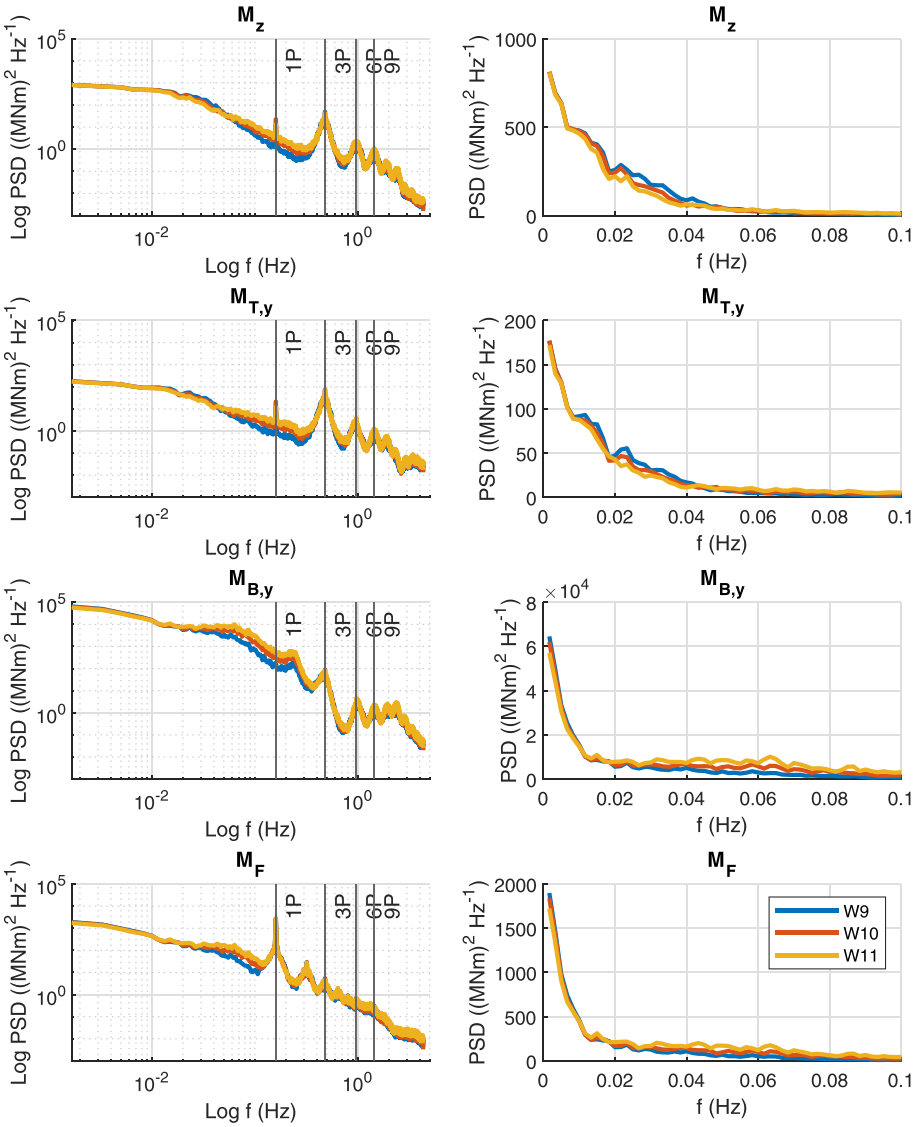

FIGURE 13 Response spectra of wind turbine response using wind fields W9–W11 of Table 4. Responses plotted using double logarithmic scale to the left; to the right the low-frequency response ($f < 0.1$ Hz) is plotted using linear scales. The mean spectra of six 1-hr realizations are shown. PSD = power spectral densities. Frequency step, $\Delta f = 0.0017$ Hz

influence the spectral densities at frequencies even higher than 0.1 Hz. This indicates that the co-coherence on length scales much smaller than the rotor diameter influences the responses. By comparing Figures 3 and 4, one observes that as the separation distance is reduced, the coherence persists at higher frequencies. Considering the DEM of the complete response time series, using the absolute value of the co-coherence (W11), rather than ignoring the negative values of co-coherence (W10) or keeping the negative values (W9), leads to higher DEM values for all considered responses. The differences are in the order of 10% for M_z, $M_{T,y}$ and M_F, while the $M_{B,y}$ is increased by 50% when the negative co-coherence is replaced by the absolute value. It may be assumed that the negative co-coherence present in Mann, being similar to W9, alters the wind turbine response as compared to coherence formulations that contain positive co-coherence only.

The coherence of the across wind and vertical wind components may also influence the loads. The effects of these components of the wind field are not analysed in the present study.

3.4 | Modelling of the low-frequency region

Above, it is shown that the low-frequency region is important for the structural damage. The IEC recommendation on the number of realizations of the simulations is furthermore considered to be too uncertain for comparing the DEM of using various input wind fields in this region. Further, the possible influence of shear, turbulence and coherence on the response is analysed. In the following, focus will be upon the response in the low-frequency region, that is, response at frequencies less than the first natural frequency of the tower and less than 1P. The response using wind fields generated by TIMESR, LES, Mann and Kaimal are considered.

The computed responses of SIMA simulations with the various wind fields are low-pass filtered and the DEM calculated. The results are presented in Figure 8 and Figure 14. The variation of the six realizations of 1 hr at 12.5 m/s are shown for all wind fields except for LES.

Figure 8 shows that, as the dynamic thrust force is highest at the rated wind speed, so are the DEM at the blade root and tower bottom. The local moments at the tower top, on the other hand, keep increasing with increasing wind speed. Only one realization is run for the above and below rated wind speed, so the results of these situations should thus not be used for comparisons across models where the results are very similar.

The response spectra, see Figures 7,15 and 16, show the frequency dependent response using the three stability situations at 12.5 m/s. It is obvious both from the DEM and the spectral response that the stable situation cause less dynamic loads. The responses of the unstable and neutral situations are rather similar, reflecting the similarities of the two chosen situations. None of the wind field models cause consistently the highest or lowest DEM throughout the responses and stability conditions considered.

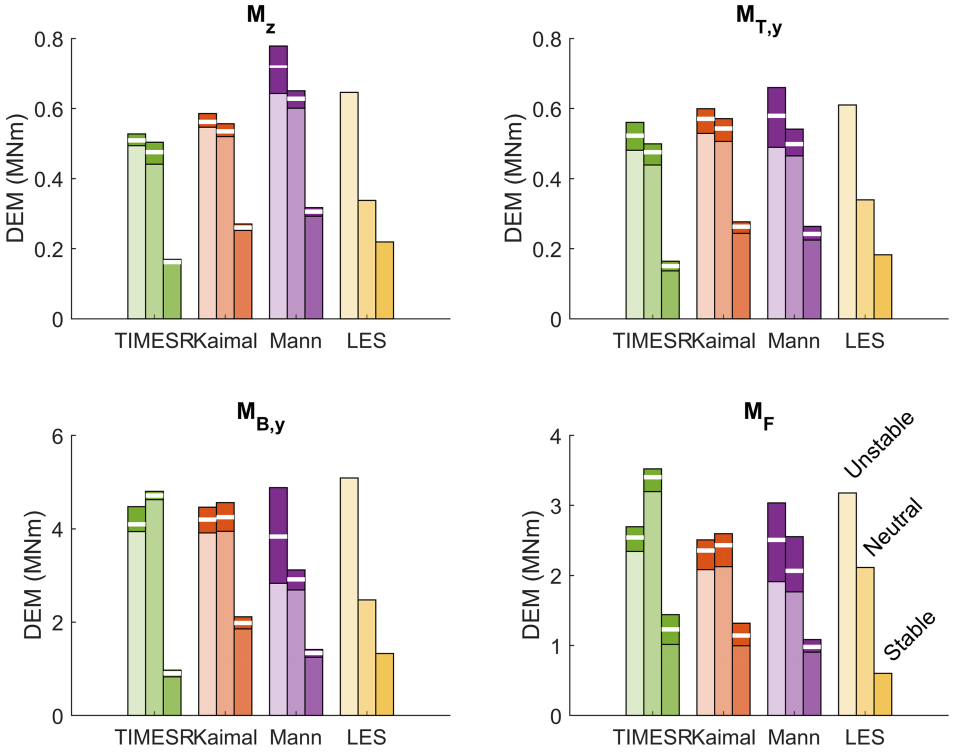

FIGURE 14 Damage equivalent moments of the low-pass filtered response time series for three input stability conditions at 12.5 m/s. The range (dark) and mean (white lines) of six 1-hr realizations are shown

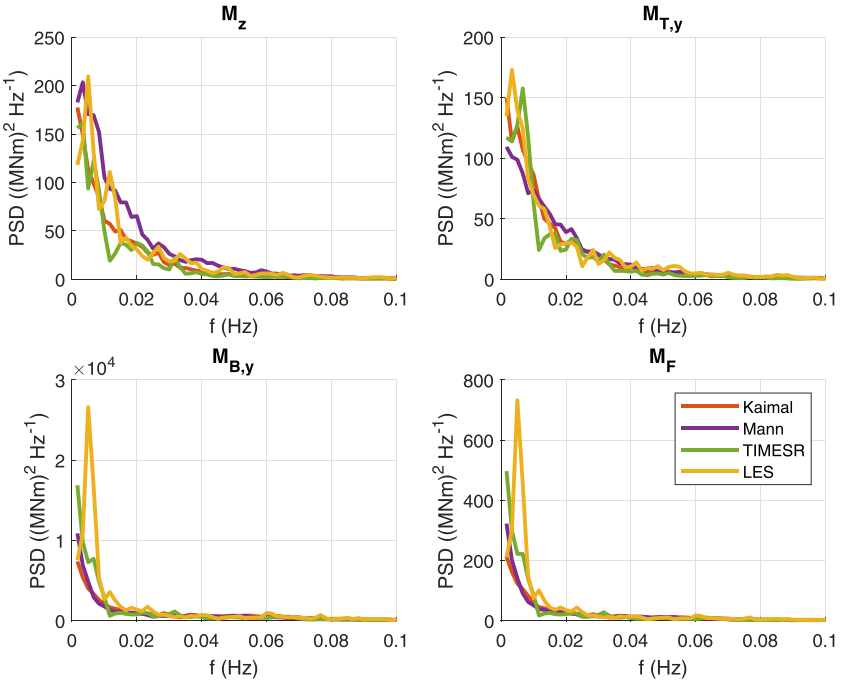

FIGURE 15 Response spectra of the wind turbine subject to wind fields of 12.5 m/s and unstable atmospheric conditions. The mean spectra of six 1-hr realizations are shown. PSD = power spectral densities. Frequency step, $\Delta f = 0.0017$ Hz

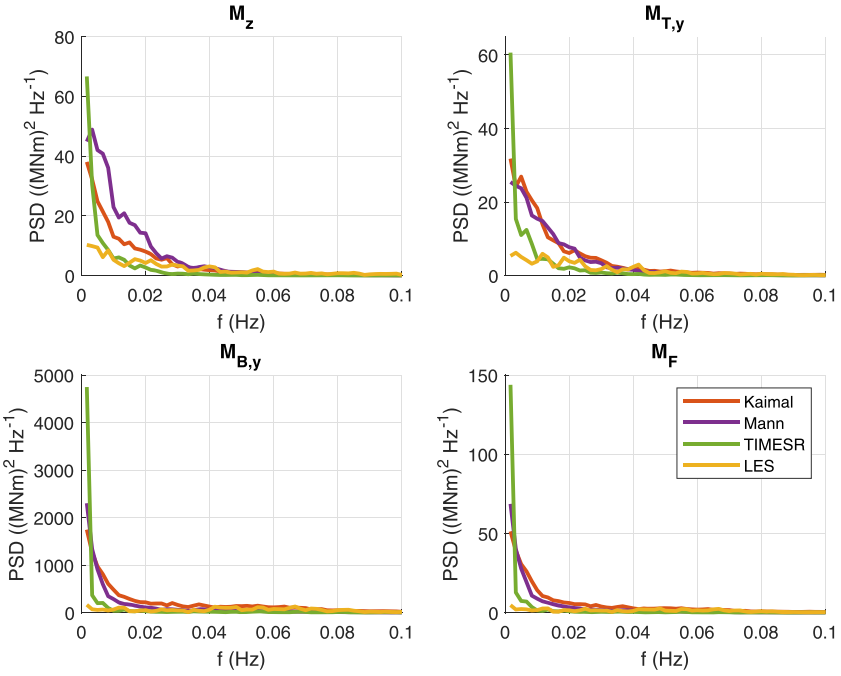

FIGURE 16 Response spectra of the wind turbine subject to wind fields of 12.5 m/s and stable atmospheric conditions. The mean spectra of six 1-hr realizations are shown. PSD = power spectral densities. Frequency step, $\Delta f = 0.0017$

In agreement with Section 3.3, one sees that the TI has a strong impact on response. The LES wind field has a very low TI in the neutral situation, which is reflected in all the DEM and spectral responses, especially in the frequency range 0.005–0.03 Hz.

It is also clear that the shape of the wind spectra have great impact on the response. In the unstable situation, a distinct behaviour of LES across the spectral responses is again obvious. In contrast to the responses of other input wind fields, LES predicts a peak in response at a frequency higher than 0.0017 Hz (lowest frequency in spectrum). The same shift of energy towards higher frequencies is seen in the wind spectra

(Figure 2, left). For the stable situation (Figure 16), one observes that the responses in the LES wind field are lower than in the other wind fields. This is a consequence of the lower spectral densities of the wind spectra, see Figure 2. However, the co-coherence of LES in the stable situation is also very low, being close to zero for most frequencies (Figure 3). As illustrated in Figure 10, low coherence at small separation distances are associated with small uncorrelated eddies, which will contribute to overall low dynamic moments. The low coherence of TIMESR at frequencies above 0.0017 Hz in the stable situation (Figure 3), cause corresponding low responses of the TIMESR input wind field. TIMESR and LES take the atmospheric stability conditions in the wind modelling into account to a larger extent than Kaimal and Mann. In contrast to Kaimal and Mann, where only the TI and shear are adapted when they are referred to as stable or unstable, TIMESR and LES adapt also the turbulence and coherence to the given stability. This seems to greatly impact the quasi-static response in the stable situation.

Considering all models and stability conditions, the Mann wind fields result in highest DEM of M_z. The spectral amplitudes of M_z in Mann are significantly higher at frequencies below 0.045 Hz compared to the spectral amplitudes in other wind fields (Figure 7,15 and 16 (all left top)). This is expected considering its low horizontal co-coherence, see Section 3.3, Putri et al.[12] and Doubrawa et al.[11] The wind fields W4 and W6 demonstrate that wind fields with low horizontal co-coherence cause high yaw moments, see Figure 9 (top), which is also illustrated in Figure 10. There is, however, a very low co-coherence of TIMESR in the stable situation as well, but this does not result in a consistently high M_z. This may indicate that the negative horizontal co-coherence, present in Mann but not TIMESR, has a strong impact on M_z.

$M_{T,y}$ is expected to be influenced by the vertical co-coherence, which is similar across wind field models (Figure 3). Figures 7,15 and 16 (all right top) show that the corresponding response spectra follow each other closely with the exceptions in LES and TIMESR already mentioned.

The $M_{B,y}$ spectra (Figures 7,15 and 16 (all left bottom)) are heavily influenced by the shape of the wind spectra in unstable and neutral conditions. There are strong similarities, especially at the lowest frequencies. Figure 14 shows that higher frequencies matter for the DEM despite the high spectral densities at the very low frequencies. One, for example, observes higher spectral densities of Kaimal than Mann at higher frequencies in all stability conditions, which leads to higher total damage. From Figure 3, one observes that Mann has highest co-coherence at very low frequencies, but Kaimal at higher frequencies. Figure 9 showed that more co-coherence cause more response at the tower bottom, explaining the differences of Mann and Kaimal. This is in contradiction to the findings of Putri et al.[12] and Bachynski and Eliassen,[10] who did not see any significant effect of co-coherence on the response in Mann versus Kaimal in $M_{B,y}$. These studies are not directly comparable to the present study, as they focus on floating wind turbines subject to waves with corresponding platform movements.

The wind spectra in neutral and unstable situations seem to influence M_F even stronger (Figures 7,15 and 16 (all right bottom)). One sees clear similarities between the response spectra of $M_{B,y}$ and M_F, but the very low frequencies seems to be dominating for the DEM of M_F. When comparing the responses at low frequencies, one should keep in mind the relatively large statistical uncertainty.

4 | CONCLUSIONS

In this study, focus is on the low-frequency response of a bottom-fixed offshore wind turbine. The effect of various turbulence models are studied. First, the wind spectra and coherence of the input wind fields, Kaimal, Mann, TIMESR and LES are compared. The turbulence models are fitted to an unstable, a neutral and a stable common situation offshore. The wind characteristics of the neutral and unstable situations are found to be very similar, while the stable situation has larger shear, lower TI and less coherence.

Next, the importance of the low-frequency, quasi-static response for some key response quantities is evaluated. The responses considered cover the tower top yaw moment, the tower top fore-aft bending moment, the tower bottom fore-aft bending moment and the blade root flapwise bending moment. The quasi-static response is shown to have a significant contribution to the DEM of these responses. The importance of the low-frequency region is higher at the tower bottom and blade root than at the tower top.

The stochastic variation of the response is furthermore evaluated with a focus on the quasi-static frequency region. The number of realizations of simulations recommended by the IEC is considered to be too uncertain for the present analysis. A total of 6 hr wind field simulations are therefore performed for Kaimal, Mann and TIMESR in order to simulate the response.

In order to identify the reasons for the differences in responses using Kaimal, Mann, TIMESR and LES, the impacts of shear, turbulence and coherence on response are analysed separately. Shear is found to have negligible impact in the low-frequency region, while increased turbulence level generally increases the response in the whole frequency range. With increasing co-coherence, the tower top yaw and bending moments are reduced, while the tower bottom and blade root bending moments are increased. The quad-coherence has negligible impact on the response parameters considered.

In this study, the wind shear, TI and wind spectra of Kaimal and Mann are alike, yet there are significant differences in response. These are explained by the differences in turbulence and coherence formulations. The co-coherence of Mann is low compared to Kaimal, even negative at some frequencies. This explains the lower response in Mann wind compared to Kaimal at the tower bottom and blade root. It is likely that the high yaw response in Mann is also related to its low and negative co-coherence, specifically between horizontal separation distances.

In agreement with the literature, this study shows that the response of the structure in Kaimal and Mann differ. Compared to the other considered models, LES and TIMESR, however, Kaimal and Mann give quite similar results. TIMESR, for example, stands out giving high DEM in the

tower bottom and blade root in the neutral and unstable situations. The shape of the response spectra of the tower bottom and blade root bending moments are similar to the wind spectra in these situations. Compared to other wind fields, TIMESR has very large spectral amplitudes in the lowest considered frequencies, which is reflected in the response spectra. In other words, the large variation in wind speed of large eddies observed in TIMESR cause high DEM at the tower bottom and blade root.

Compared to Mann, Kaimal and TIMESR, the wind characteristics of LES and the corresponding response differ distinctively with stability. LES has different input parameters, more complex formulations and severely increased computational costs compared to the other models. As the TI, wind shear and coherence are resulting parameters rather than inputs, it is more difficult to customize the simulations to certain situations. As an example, obtaining high enough TI in the neutral situation was difficult, which dominated the corresponding response.

The largest differences between models are found in the stable situation. In contrast to Mann and Kaimal, there are clear dependencies of stability on the response spectra of TIMESR and LES. The low response of LES and TIMESR in stable conditions is expected to be related to few energetic large eddies and corresponding insignificant forces.

The four wind field models result in large differences in the estimated DEM of the quasi-static response even when all models are fit to the same offshore situation. Thus, the choice of turbulence model is important to the fatigue life estimates in design of bottom-fixed wind turbines. A correct modelling of turbulence and coherence becomes more important with increasing rotor diameters. It is not possible to conclude which turbulence model is superior, as no full field measurements are included in the study. This study shows that the horizontal coherence impacts the response, but measurements of the actual horizontal coherence are rare.

Further work will include fitting the input parameters of the Mann model to measured data. The characteristics of the Mann wind field, such as the eddy size and lifetime may thus be fitted to given situations. Furthermore, studies will be performed on a floating wind turbine subject to the wind fields used in this study. With its low natural frequencies of the rigid body motions, even higher significance of the low-frequency region of the response spectrum is expected. The differences between the response of various wind fields are thus expected to be even clearer.

ACKNOWLEDGEMENTS

The authors would like to thank Maylinn Haaskjold Myrtvedt for cooperation on the bottom-fixed wind turbine. Her recent paper was a great inspiration source for this work. We would also like to thank Stian Høegh Sørum for sharing his bottom-fixed DTU wind turbine model and experience with the model with us. For providing LES wind fields and associated support, we would like to thank Matthew J. Churchfield at the National Renewable Energy Laboratory. A portion of the research was performed using computational resources sponsored by the Department of Energy's Office of Energy Efficiency and Renewable Energy and located at the National Renewable Energy Laboratory. We would like to thank Etienne Cheynet, our colleague at the Geophysical Institute, for his support on coherence modelling. Last, we would like to thank Joachim Reuder, also our colleague at the Geophysical Institute, for his support on a prior wind field study which paved the way for this work.

PEER REVIEW

The peer review history for this article is available at https://publons.com/publon/10.1002/we.2642.

DATA AVAILABILITY STATEMENT

The data that support the findings of this study are available from the corresponding author upon reasonable request.

ORCID


Astrid Nybø https://orcid.org/0000-0002-7438-7936

REFERENCES

1. Lee J, Zhao F, Dutton A, et al. Global offshore wind report 2020. tech. rep., Brussels: GWEC; 2020. https://gwec.net/global-offshore-wind-report-2020/. Accessed February 16, 2021.
2. International Electrotechnical Commision. IEC 61400-1 Wind energy generation systems—Part 1: Design requirements. tech. rep., Geneva: IEC; 2019. https://webstore.iec.ch/publication/26423. Accessed February 16, 2021.
3. International Electrotechnical Commision. IEC 61400-3-1:2019 Wind energy generation systems—Part 3-1: Design requirements for fixed offshore wind turbines. tech. rep., Geneva: IEC; 2019. https://webstore.iec.ch/publication/29360. Accessed February 16, 2021.
4. International Electrotechnical Commision. IEC TS 61400-3-2:2019 Wind energy generation systems - Part 3-2: Design requirements for floating offshore wind turbines. tech. rep., Geneva: IEC; 2019. https://webstore.iec.ch/publication/29244. Accessed February 16, 2021.
5. Mann J. The spatial structure of neutral atmospheric surface-layer turbulence. *J Fluid Mech*. 1994;273:141-168.
6. Kaimal JC, Wyngaard JC, Izumi Y, Coté OR. Spectral characteristics of surface-layer turbulence. *Q J Roy Meteor Soc*. 1972;98(417):563-589.
7. Myrtvedt MH, Nybø A, Nielsen FG. The dynamic response of offshore wind turbines and their sensitivity to wind field models. *J Phys Conf Ser*. 2020;1669:12013.
8. Eliassen L, Bachynski EE. The effect of turbulence model on the response of a large floating wind turbine. In: *ASME 2017 36th Int Conf Ocean, Offshore and Arctic Engineering*. Trondheim, Norway; 2017:1-10. https://doi.org/10.1115/OMAE2017-61179

9. Godvik M. Influence of wind coherence on the response of a floating wind turbine. In: *Science meets Industry*. Stavanger, Norway; 2016:1-12. http://www.norcowe.no/doc//konferanser/2016/SMIStavangerpresentasjoner/GodvikStatoilInfluenceofthewindcoherenceontheresponseofafloatingwindturbine.pdf
10. Bachynski EE, Eliassen L. The effects of coherent structures on the global response of floating offshore wind turbines. *Wind Energy*. 2019;22(2):219-238.
11. Doubrawa P, Churchfield MJ, Godvik M, Sirnivas S. Load response of a floating wind turbine to turbulent atmospheric flow. *Appl Energ*. 2019;242:1588-1599. https://doi.org/10.1016/j.apenergy.2019.01.165
12. Putri RM, Obhrai C, Jakobsen JB, Ong MC. Numerical analysis of the effect of offshore turbulent wind inflow on the response of a spar wind turbine. *Energies*. 2020;13(10):1-22. https://doi.org/10.3390/en13102506
13. Putri RM, Obhrai C, Knight JM. Offshore wind turbine loads and motions in unstable atmospheric conditions. *J Phys Conf Ser*. 2019;1356:12016.
14. Holtslag MC, Bierbooms WM, van Bussel GJW. Wind turbine fatigue loads as a function of atmospheric conditions offshore. *Wind Energy*. 2016;19(10):1917-1932.
15. Hanssen-Bauer W, de Vaal JB, Tutkun M, Asmuth H, Ivanell S, Stenbro R. Dependence of wind turbine loads on inlet flow field. *J Phys Conf Ser*. 2020;1618:62065.
16. Argyriadis K. Validation of turbulence models - DNV GL. https://www.dnvgl.com/cases/validation-of-turbulence-models-86603. Accessed February 16, 2021; 2016.
17. Eliassen L, Jakobsen JB, Obhrai C. The effect of atmospheric stability on the fatigue life of offshore wind turbines. In: *Proc 22nd Int Offshore and Polar Engineering Conf*. Rhodes, Greece; 2012:330-336. https://www.onepetro.org/conference-paper/ISOPE-I-12-206
18. Nybø A, Nielsen FG, Reuder J, Churchfield M, Godvik M. Evaluation of different wind fields for the investigation of the dynamic response of offshore wind turbines. *Wind Energy*. 2020;23(9):1810-1830.
19. FuE-Zentrum FH Kiel GmbH. FINO1: Forschungsplattformen in Nord- und Ostsee Nr. 1. http://www.fino1.de/en/. Accessed February 16, 2021; 2019.
20. Nybø A, Nielsen FG, Reuder J. Processing of sonic anemometer measurements for offshore wind turbine applications. *J Phys Conf Ser*. 2019;1356:12006.
21. Jonkman BJ. TurbSim User's Guide v2.00.00. tech. rep., Golden: NREL; 2016.
22. Davenport AG. The spectrum of horizontal gustiness near the ground in high winds. *Q J Roy Meteor Soc*. 1961;87(372):194-211.
23. Kristiansen MB. Mann 64bit turbulence generator. https://www.hawc2.dk/download/pre-processing-tools. Accessed February 16, 2021; 2018.
24. Churchfield M, Lee S, Moriarty P. Overview of the Simulator fOr Wind Farm Application (SOWFA). tech. rep., NREL; 2012. https://www.nrel.gov/wind/nwtc/assets/pdfs/sowfa-tutorial.pdf. Accessed February 16, 2021.
25. Robertson A, Sethuraman L, Jonkman J, Quick J. Assessment of wind parameter sensitivity on ultimate and fatigue wind turbine loads. NREL/CP-5000-70445, NREL; 2018. https://www.nrel.gov/docs/fy18osti/70445.pdf. Accessed February 16, 2021.
26. Shaler K, Jonkman J, Doubrawa P, Hamilton N. FAST.farm response to varying wind inflow techniques. NREL/CP-5000-72893, NREL; 2019. https://www.nrel.gov/docs/fy19osti/72893.pdf. Accessed February 16, 2021.
27. Veers PS. Three-dimensional wind simulation, Sandia National Laboratories; 1988. https://prod-ng.sandia.gov/techlib-noauth/access-control.cgi/1988/880152.pdf. Accessed February 16, 2021.
28. Eliassen L, Obhrai C. Coherence of turbulent wind under neutral wind conditions at FINO1. *Enrgy Proced*. 2016;94:388-398.
29. Saranyasoontorn K, Manuel L, Veers PS. A comparison of standard coherence models for inflow turbulence with estimates from field measurements. *J Sol Energ-T ASME*. 2004;126(4):1069-1082.
30. Bak C, Zahle F, Bitsche R, et al. The DTU 10-MW reference wind turbine. tech. rep., DTU; 2013. http://orbit.dtu.dk/ws/files/55645274/The_DTU_10MW_Reference_Turbine_Christian_Bak.pdf. Accessed February 16, 2021.
31. Bachynski EE, Ormberg H. Hydrodynamic modeling of large-diameter bottom-fixed offshore wind turbines. In: *Proc Int Conf OMAE*. St. John's, Newfoundland, Canada; 2015:1-9. https://doi.org/10.1115/OMAE2015-42028
32. Sørum SH, Krokstad JR, Amdahl J. Wind-wave directional effects on fatigue of bottom-fixed offshore wind turbine. *J Phys Conf Ser*. 2019;1356:12011.
33. Hermundstad OA. Sima—SINTEF. https://www.sintef.no/programvare/sima/. Accessed February 16, 2021.
34. Welch PD. The use of fast Fourier transform for the estimation of power spectra: A method based on time averaging over short, modified periodograms. *IEEE Trans Audio Electroacoust*. 1967;15(2):70-73.
35. International Electrotechnical Commision. IEC TS 61400-13: wind turbine generator systems—Part 13: Measurement of mechanical loads. tech. rep., IEC; 2015. https://webstore.iec.ch/publication/23971. Accessed February 16, 2021.
36. Niesłony A. Determination of fragments of multiaxial service loading strongly influencing the fatigue of machine components. *Mech Syst Signal Pr*. 2009;23(8):2712-2721.
37. Stewart G, Lackner M, Haid L, Matha D, Jonkman J, Robertson A. Assessing fatigue and ultimate load uncertainty in floating offshore wind turbines due to varying simulation length. In: *Proc 11th Int Conf Structural Safety and Reliability, ICOSSAR 2013*. New York, United States; 2013:1-8. https://doi.org/10.1201/b16387-33
38. Bergami L, Gaunaa M. Analysis of aeroelastic loads and their contributions to fatigue damage. *J Phys Conf Ser*. 2014;555:12007.
39. Bendat JS, Piersol AG. *Random Data: Analysis and Measurement Procedures*. California, United States: John Wiley & Sons; 1971.
40. Cheynet E. Wind field simulation (the fast version). https://doi.org/10.5281/ZENODO.3774136. Accessed Feburary 16, 2021; 2020.
41. Cheynet E, Jakobsen JB, Snæbjörnsson J, et al. Application of short-range dual-Doppler lidars to evaluate the coherence of turbulence. *Exp Fluids*. 2016;57:1-17.

How to cite this article: Nybø A, Nielsen FG, Godvik M. Quasi-static response of a bottom-fixed wind turbine subject to various incident wind fields. *Wind Energ*. 2021;24(12):1482-1500. https://doi.org/10.1002/we.2642